Draft version September 16, 2020
Typeset using LaTeX **twocolumn** style in AASTeX63

SDSS-IV MaNGA: The Nature of an Off-galaxy Hα Blob – A Multi-wavelength View of Offset Cooling in a Merging Galaxy Group

Hsi-An Pan (潘璽安),[1,2] Lihwai Lin,[1] Bau-Ching Hsieh,[1] Michał J. Michałowski,[3] Matthew S. Bothwell,[4,5] Song Huang,[6,7,8] Alexei V. Moiseev,[9,10] Dmitry Oparin,[9] Ewan O'Sullivan,[11] Diana M. Worrall,[12] Sebastián F. Sánchez,[13] Stephen Gwyn,[14] David R. Law,[15] David V. Stark,[16] Dmitry Bizyaev,[17,18] Cheng Li,[19] Chien-Hsiu Lee,[20] Hai Fu,[21] Francesco Belfiore,[22] Kevin Bundy,[23] José G. Fernández-Trincado,[24] Joseph Gelfand,[25,26] and Sébastien Peirani[27,28]

[1] *Institute of Astronomy and Astrophysics, Academia Sinica, No. 1, Section 4, Roosevelt Road, Taipei 10617, Taiwan*
[2] *Max-Planck-Institut für Astronomie, Königstuhl 17, D-69117 Heidelberg, Germany*
[3] *Astronomical Observatory Institute, Faculty of Physics, Adam Mickiewicz University, ul. Słoneczna 36, 60-286 Poznań, Poland*
[4] *Cavendish Laboratory, University of Cambridge, 19 J. J. Thomson Avenue, Cambridge CB3 0HE, UK*
[5] *University of Cambridge, Kavli Institute for Cosmology, Cambridge, CB3 0HE, UK*
[6] *Department of Astronomy and Astrophysics, University of California Santa Cruz, 1156 High St., Santa Cruz, CA 95064, USA*
[7] *Kavli-IPMU, The University of Tokyo Institutes for Advanced Study, the University of Tokyo*
[8] *Department of Astrophysical Sciences, Peyton Hall, Princeton University, Princeton, NJ 08540, USA*
[9] *Special Astrophysical Observatory, Russian Academy of Sciences, Nizhnij Arkhyz, 369167, Russia*
[10] *Space Research Institute, Russian Academy of Sciences, Profsoyuznaya ul. 84/32, Moscow 117997, Russia*
[11] *Harvard-Smithsonian Center for Astrophysics, 60 Garden Street, Cambridge, MA 02138, USA*
[12] *HH Wills Physics Laboratory University of Bristol, Tyndall Avenue, Bristol BS8 1TL, UK*
[13] *Instituto de Astronomía, Universidad Nacional Autónoma de México, A. P. 70-264, C.P. 04510, México, D.F., Mexico*
[14] *NRC-Herzberg Astronomy and Astrophysics, National Research Council of Canada, 5071 West Saanich Road, Victoria, British Columbia V9E 2E7, Canada*
[15] *Space Telescope Science Institute, 3700 San Martin Drive, Baltimore, MD 21218, USA*
[16] *Physics and Astronomy, Haverford College, Haverford, PA*
[17] *Apache Point Observatory and New Mexico State University, Sunspot, NM, 88349, USA*
[18] *Sternberg Astronomical Institute, Moscow State University, Moscow, Russia*
[19] *Tsinghua Center of Astrophysics & Department of Physics, Tsinghua University, Beijing 100084, China*
[20] *NSF's National Optical-Infrared Astronomy Research Laboratory, Tucson, AZ, USA*
[21] *Department of Physics & Astronomy, University of Iowa, Iowa City, IA 52242, USA*
[22] *European Southern Observatory, Karl-Schwarzchild-Str. 2, Garching bei Mnchen, D-85748, Germany*
[23] *Department of Astronomy and Astrophysics, University of California, Santa Cruz, 1156 High Street, Santa Cruz, CA 95064, USA*
[24] *Instituto de Astronomía y Ciencias Planetarias, Universidad de Atacama, Copayapu 485, Copiapó, Chile*
[25] *NYU Abu Dhabi, United Arab Emirates*
[26] *NYU Center for Cosmology and Particle Physics, New York, NY 10003, USA*
[27] *Université Côte d'Azur, Observatoire de la Côte d'Azur, CNRS, Laboratoire Lagrange, Nice, France*
[28] *Institut d'Astrophysique de Paris, CNRS & UPMC, UMR 7095, 98 bis Boulevard Arago, F-75014 Paris, France*

(Received; Revised; Accepted)

Submitted to

ABSTRACT

Galaxies in dense environments, such as groups and clusters, experience various processes by which galaxies gain and lose gas. Using data from the SDSS-IV MaNGA survey, we previously reported the discovery of a giant (6 – 8 kpc in diameter) Hα blob, Totoro, about 8 kpc away from a pair of galaxies (Satsuki and Mei) residing in a galaxy group which is experiencing a group-group merger. Here, we combine interferometric ^{12}CO(1–0) molecular gas data, new wide-field Hα, u-band data, and

Corresponding author: Hsi-An Pan
pan@mpia.de

published X-ray data to determine the origin of the blob. Several scenarios are discussed to account for its multi-wavelength properties, including (1) Hα gas being stripped from galaxy Satsuki by ram-pressure; (2) a separated low-surface-brightness galaxy; (3) gas being ejected or ionized by an active galactic nucleus (AGN); and (4) a cooling intra-group medium (IGM). Scenarios (1) and (2) are less favored by the present data. Scenario (3) is also less likely as there is no evidence for an active ongoing AGN in the host galaxy. We find that the CO (cold) and Hα (warm) gas coexist with X-ray (hot) structures; moreover, the derived cooling time is within the regime where molecular and Hα gas are expected. The coexistence of gas with different temperatures also agrees with that of cooling gas in other systems. Our multi-wavelength results strongly suggest that the CO and Hα gas are the product of cooling from the IGM at its current location, i.e., cooling has occurred, and may be ongoing, well outside the host-galaxy core.

Keywords: galaxies: evolution — galaxies: groups — galaxies: interactions — galaxies: intergalactic medium — galaxies: peculiar

1. INTRODUCTION

The optical colors of galaxies are characterized by a bimodality, with early-type galaxies residing on the red sequence and late-type galaxies populating the blue cloud (e.g., Strateva et al. 2001; Balogh et al. 2004; Brammer et al. 2009). The transition from blue to red galaxies is known to be driven by a decrease in star formation (e.g., Whitaker et al. 2012; Taylor et al. 2015). Since galaxies require gas to fuel star formation (e.g., Saintonge et al. 2017), a knowledge of the gain and loss of gas provides a huge leap in the understanding of galaxy evolution.

Many galaxies reside in gravitationally bound groups or clusters, where a high volume density of galaxies is found. A natural consequence of clustering of galaxies is frequent interactions between galaxies and the environment in which they live (e.g., Fernández-Trincado et al. 2014). Such interactions can stimulate the gain and loss and heating and cooling of gas in various ways and control the star formation processes in galaxies. For example, interaction between galaxies can potentially trigger nuclear activity and nuclear starbursts that generate energetic gas outflow/winds to the environments (e.g., Larson, & Tinsley 1978; Silk, & Rees 1998; Springel et al. 2005; Ellison et al. 2008; Hopkins et al. 2008; Fernández-Trincado et al. 2014). Besides, when a galaxy moves at a high speed through a high density region, a complex hydrodynamical interaction of its interstellar medium (ISM) and the surrounding hot intracluster/intergalactic medium takes place. A large fraction of gas could be removed from a galaxy if the ram-pressure is strong enough to overcome the gravitational force (Gunn, & Gott 1972). These gas removal processes can lead to the interruption of star formation activity.

On the other hand, fresh supplies of gas can sustain star formation in galaxies. Galaxies can gain gas through accretion of small companions (Bond et al. 1991; Lacey & Cole 1993). Moreover, cold gas can form from the cooling of the hot intracluster medium (ICM) or intragroup medium (IGM) and be accreted to galaxies (Egami et al. 2006; O'Dea et al. 2008). Such process can rejuvenate early-type and S0 galaxies by supplying gas into their centers.

In our previous paper, Lin et al. (2017, hereafter Paper I), we report the discovery of a giant ionized gaseous (Hα) blob associated with a dry merger system (i.e., mergers between two early-type galaxies; Figure 1a and 1b) residing in a galaxy group (Figure 1c). The ionized gaseous blob is offset from both of the galactic nuclei. The gaseous blob might be a result of galaxy interactions, active galactic nucleus (AGN) activity, or a galaxy interacting with or being accreted by the dry merger. In any of these cases, we may be witnessing an ongoing gain and/or loss of gas in these galaxies.

The Hα blob was identified from the first-year MaNGA survey (Mapping Nearby Galaxies at APO; Bundy et al. 2015), part of SDSS-IV (Blanton et al. 2017). The Hα blob (nicknamed "Totoro") is $\sim$ 3 – 4 kpc in radius and is $\sim$ 8 kpc away (in projection) from the host galaxy MaNGA target 1-24145 (or MCG+10-24-117; nicknamed "Satsuki"; $17^{\rm h}15^{\rm h}23.26^{\rm s}$, $+57°25'58.36''$, stellar mass $M_* \approx 10^{11}$ $M_\odot$). There is no distinct optical continuum counterpart at the position of Totoro. The mass of the ionized gas is 8.2×10^4 $M_\odot$ (Paper I). The SDSS image indicates that the host galaxy Satsuki has a companion galaxy (nicknamed "Mei") located to the south east of Satsuki (Figure 1b). The companion is also within the hexagon bundle field of view (FoV; $\sim 32.5''$ in diameter) of MaNGA. These two galaxies are at similar redshifts ($z \approx 0.03$), with their line of sight velocity differing by $\sim$ 200 km s^{-1}. Both galaxies are elliptical and thus form a dry (gas-poor) merger, also known as VII Zw 700.

On the large scale, the dry merger (Satsuki and Mei) is located at the overlap region of a group-group merger

(O'Sullivan et al. 2019). Satsuki and Mei are associated with the less massive northern component, while the nearby large elliptical galaxy NGC 6338 is the brightest galaxy of the more massive group (Figure 1c). The dry merger (Satsuki and Mei) and NGC 6338 are separated by $\sim$ 42 kpc in projection and by $\sim$ 1400 km s^{-1} in velocity. The two merging groups are expected to form a galaxy cluster in the future. The merger velocity of the two groups is as large as 1700 – 1800 km s^{-1}, making this one of the most violent mergers yet observed between galaxy groups (O'Sullivan et al. 2019).

Our Hα blob Totoro has also been observed by O'Sullivan et al. (2019) using the APO 3.5-m telescope (see their Figure 10), but only the high-luminosity, main blob region was detected. O'Sullivan et al. (2019) also show that the Hα gas of NGC 6338 consists of three diffuse filaments in the southeast and northwest quadrants, extending out to $\sim$ 9 kpc from the nucleus. The Hα filaments have also been revealed in previous observations by *HST* and the CALIFA[1] survey (Martel et al. 2004; Pandge et al. 2012; Gomes et al. 2016). Moreover, O'Sullivan et al. (2019) show that both NGC 6338 and VII Zw 700 contain potential X-ray cavities, which would indicate past AGN jet activity. In addition, both systems are observed to contain cool IGM structures correlated with the Hα emission (see also Pandge et al. 2012).

We diagnosed the physical properties of Satsuki and Tororo using MaNGA data in Paper I:

- *kinematics*: the ionized (Hα) gas component reveals that there is a moderate velocity variation ($\leqslant$ 100 km s^{-1}) from the position of Satsuki along the connecting arms to Totoro, but there is no velocity gradient across Totoro itself and the velocity and velocity dispersion across the blob are low ($\ll$ 100 km s^{-1}; Figure 7 of Paper I).

- *excitation state*: the Baldwin-Phillips-Terlevich (BPT) emission line diagnostics (Baldwin et al. 1981) indicate LI(N)ER-type excitations for Satsuki and a composite (LI(N)ER-HII mix[2]) for Totoro.

- *gas metallicity*: metallicity[3] of the gas around Satsuki is close to the solar value; on the other hand, the metallicity of Totoro is higher than that of Satsuki by 0.3 dex.

Several possibilities for Totoro were raised in Paper I, including (1) the gas being ram-pressure stripped from Satsuki, (2) a galaxy interacting with the dry merger (Satsuki and Mei), and (3) gas being ejected or ionized by an AGN associated with Satsuki. However, the data in Paper I are not sufficient to provide strong constraints on the nature of Totoro.

In this paper, we present new observations of this system and determine the most plausible origin of Totoro. Our new observations include:

(i) *wide-field Hα image*: to reveal the distribution of ionized gas at larger scale (i.e., beyond the FoV of the MaNGA bundle),

(ii) *u-band observation*: to constrain the ionizing source, i.e., star formation or not, and to search for the possible continuum counterpart of the Hα blob, and

(iii) *molecular gas in ^{12}CO(1–0)*: to constrain the amount and distribution of cold, i.e., potentially star-forming, gas.

Moreover, in addition to the scenarios raised in Paper I, O'Sullivan et al. (2019) argue for the "cooling gas" hypothesis in Satsuki, therefore, we also use

(iv) *X-ray data* from O'Sullivan et al. (2019) to constrain the properties of the surrounding hot medium.

The paper is organized as follows. Section 2 describes the observations and our data reduction. The results are presented and discussed in Section 3. In Section 4 we summarize our results and list our conclusions.

Throughout this study, we assume a cosmology with $\Omega_{\rm m} = 0.3$, $\Omega_\Lambda = 0.7$, and $H_0 = 70$ km s^{-1} Mpc^{-1}. We use a Salpeter stellar initial mass function.

2. DATA

2.1. *MaNGA*

[1] Calar Alto Legacy Integral Field Area Survey (Sánchez et al. 2012).

[2] Shocks can also lead to line ratios occupying the composite regions. However, the analysis of shock and photoionization mixing models of Paper I shows that the shocks are unlikely to be the dominant mechanism that is responsible for ionization of Totoro.

[3] Most of the metallicity calibrators can only be applied for those regions in which ionization is dominated by star formation, and may not be applicable to regions with ionization parameters or ISM pressure different from typical HII regions. In Paper I, we adopted the "N2S2Hα" calibrator, which is suggested to be less sensitive to the ionization parameters (Dopita et al. 2016). However, caution is still needed when interpreting the derived metallicity.

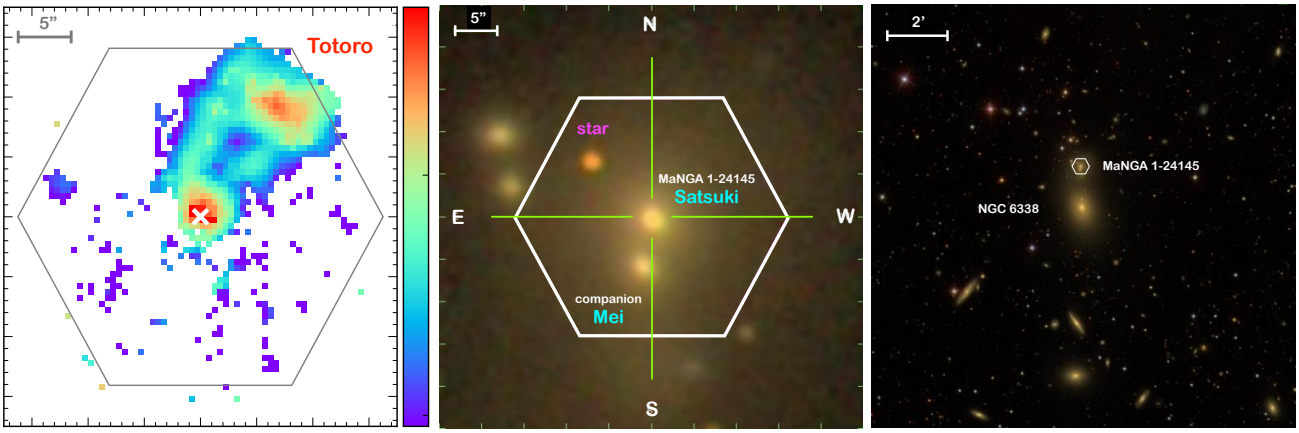

Figure 1. Optical images of MaNGA 1-24145 (nicknamed “Satsuki”) and the environment in which it lives. The hexagons show the coverage of MaNGA bundle field of view. Satsuki was observed with the 127 fiber bundle of MaNGA; the hexagon is $\sim 32.5''$ in diameter. (a) MaNGA Hα map of MaNGA 1-24145. An Hα blob (nicknamed “Totoro”) is about 8 kpc northwest of MaNGA 1-24145. The unit of the map is 10^{-16} erg s^{-1} cm^{-2}. The data extend to regions just outside the hexagon because of the dithering. (b) The SDSS *gri* composite image centering on MaNGA 1-24145. The south companion (nicknamed “Mei”) is also within the MaNGA field of view. (c) The SDSS *gri* composite image of MaNGA 1-24145 and the nearby galaxies.

MaNGA, the largest integral field spectroscopy (IFS) survey of the nearby Universe to date, observed $\sim$ 10,000 galaxies with a median redshift (z) of 0.03. The details of the MaNGA survey, the integral-field-unit (IFU) fiber system, the sample selection, observing strategy, and the data reduction and analysis pipelines are explained in Drory et al. (2015), Wake et al. (2017), Law et al. (2015), Law et al. (2016), and Westfall et al. (2019), respectively, and also summarized in Paper I.

The MaNGA data used in this work were reduced using the MPL-7 version (corresponding to SDSS data release 15, Aguado et al. 2019) of the MaNGA data reduction pipeline. An earlier version of the pipeline (MPL-4) was used for Paper I. The differences between the pipeline products of MPL-4 and MPL-7 are negligible for the current work. The spectral-line fitting is carried out using the Pipe3D pipeline (Sánchez et al. 2016a,b). Details of the fitting procedures are described in Sánchez et al. (2016a,b) and summarized in Paper I. The method described in Vogt et al. (2013) is used to compute the reddening using the Balmer decrement at each spaxel.

2.2. *Wide-field Hα data*

Deep optical images were taken at the prime focus of the 6-m telescope of the Special Astrophysical Observatory of the Russian Academy of Sciences (SAO RAS) with the SCORPIO-2 multimode focal reducers (Afanasiev, & Moiseev 2011). A narrow-band filter AC6775 (the central wavelength CWL = 6769Å, the bandwidth FWHM = 15Å) covers the spectral region around the redshifted Hα emission line. Two middle-band filters FN655 (CWL = 6559Å, FWHM = 97Å) and FN712 (CWL = 7137Å, FWHM = 209Å) were used to obtain the blue and red continuum images. We combined the data taken during two nights 05/06 and 06/07 Mar 2017 with seeing of 1.3 – 1.5″. The total exposure time depended on filter FWHM: 7800, 1300, and 780 sec in the filters AC6775, FN655 and FN712, respectively. The detector, CCD E2V 42-90 (2K × 4.5K), operated in the bin 2 × 2 read-out mode provides 0.35″/px scale in the 6.1′ field of view.

The data reduction was performed in a standard way for SCORPIO-2 direct image processing with IDL-based software (see, for instance, Sitnik et al. 2015). The underlying stellar continuum from the Hα image was subtracted using the linear combination of the images in the filters FN655 and FN712. The astrometry grid was created using the Astrometry.net project web-interface[4] (Lang et al. 2010).

We emphasize that the purpose of the wide-field observation is to reveal the distribution of Hα gas outside of the MaNGA FoV, in particular, to look for a potential tidal tail(s) on the other side of Totoro. To be in line with the measurements and discussions in Paper I, the MaNGA Hα map will be used by default throughout this paper, and the wide-field Hα map will be used only where specifically mentioned in the text. The flux of the new narrow-band image has been calibrated by the MaNGA spectral line data to avoid systematic errors

[4] http://nova.astrometry.net/

related with narrow-band filter calibration (e.g., only one standard star per night, mismatch between the redshifted lines and a peak of the filter transmission curve, etc.). This forces the flux of the narrow-band image to be consistent with that of MaNGA spectral line data.

2.3. *u-band Data*

The u-band observation was taken with the wide-field imaging facility MegaCam with a 1° field of view at the Canada—France—Hawaii Telescope (CFHT) from April 27th to June 24th in 2017 (PI: L. Lin; project ID: 17AT008). The total exposure time is 12,000 seconds. The MegaCam data were processed and stacked via MegaPipe (Gwyn 2008). The final image has a limiting mag of 26.3 mag (1″ aperture in radius).

2.4. *Molecular Gas (CO) Data*

We mapped the ^{12}CO($J = 1 \rightarrow 0$; 115.2712 GHz) emission with the NOrthern Extended Millimeter Array (NOEMA) at Plateau de Bure (PI: L. Lin; project ID: S16BE001). The full width at half power of the primary beam of each NOEMA antenna at the ^{12}CO(1-0) frequency is $\sim 50''$, sufficiently large to cover Satsuki, Mei, and Totoro. The observations were spread across 11 nights from May 25th to July 18th of 2015 with 5 or 7 antennas in D configuration. The total on-science-source time is ~ 22 hours. The shortest possible baseline length is ~ 24m, and therefore sources larger than about $15''$ might be resolved out. Nonetheless, in Section 3, we will see that the distribution of molecular gas matches the Hα extremely well.

Data reduction, calibration, and imaging were performed with the CLIC and MAPPING software of GILDAS[5] using standard procedures. Images were reconstructed using natural weighting to preserve maximal sensitivity. The resultant synthesized beam is $3.4'' \times 2.3''$ (PA = 73.3°), with an effective beamsize of $2.8''$. The aim of the observation is to constrain the amount of molecular gas traced by ^{12}CO(1-0), therefore a relatively low spectral resolution (53.6 km s^{-1}) was proposed to maximize the detection probability. The rms noise in the ^{12}CO(1-0) cube is 0.31 mJy beam^{-1} per 53.6 km s^{-1}.

Figure 2 shows the ^{12}CO(1-0) spectrum integrated over Totoro and the connecting arms, outlined by a dashed ellipse with an area of 210 arcsec^2 on the integrated intensity map in Figure 3a. The ^{12}CO(1-0) emission is strongly detected in two channels with velocities of $\sim 0 - 100$ km s^{-1} and marginally detected in the adjacent channels. A single Gaussian fit to the line profile is overplotted in Figure 2. The full width half maximum (FWHM) of the line is 86.5±7.4 km s^{-1} and the line velocity relative to the galaxy velocity is 18.6±3.3 km s^{-1}. The ^{12}CO(1-0) (hereafter, CO) line properties are summarized in Table 1.

[5] http://www.iram.fr/IRAMFR/GILDAS

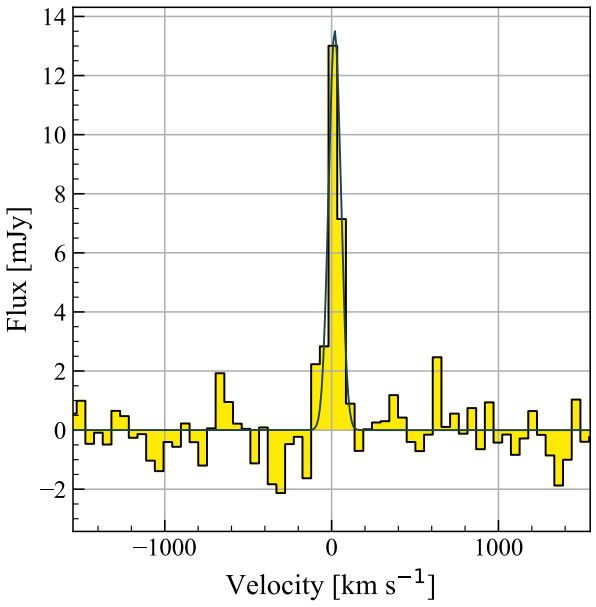

Figure 2. NOEMA ^{12}CO(1-0) spectrum integrated over the Hα blob (Totoro) and the connecting arms. The area, 210 arcsec^2, we have used for deriving the spectrum is indicated by the dashed ellipse in Figure 3a. A single Gaussian fit to the line profile is overplotted. Significant ^{12}CO(1-0) emission is detected at Totoro.

3. RESULTS AND DISCUSSION

In this section, we will present and discuss our results following the scenarios mentioned in the Introduction, namely, Section 3.1: the gas being ram-pressure stripped from Satsuki; Section 3.2: an extremely low surface brightness galaxy or ultra-diffuse galaxy; Section 3.3: gas being ejected or ionized by an AGN. In addition, Paper I did not discuss the scenario of cooling of the IGM, which we discuss in Section 3.4. We will present the analysis and results of data at a specific wavelength described in Section 2 when it is needed to test a specific scenario.

3.1. *Ram-Pressure Stripping*

Galaxies in dense environments experience ram-pressure (Gunn, & Gott 1972). As pointed out in Paper I, ram-pressure stripping is not expected to produce a centrally-concentrated blob, but is more likely to form clumpy structures embedded in a jellyfish-like tail (e.g., Boselli et al. 2016; Poggianti et al. 2017; Bellhouse et al. 2019; Jáchym et al. 2019).

Table 1. ^{12}CO (1-0) line properties of the Hα blob Totoro.

velocity (km s^{-1})	line flux (Jy)	line luminosity (K km s^{-1} pc^2)	line wdith (km s^{-1})	peak flux (mJy)
18.6±3.3	1.01±0.05	(4.83±0.23)×10^7	86.5±7.4	13.00 ± 0.74

The centrally peaked structure we observe in Totoro in Hα is also seen in molecular gas. The integrated intensity map of CO is shown in Figure 3a and the comparison with Hα is displayed in Figure 3b The morphology of molecular gas generally agrees well with Hα emission. The CO emission of Totoro is also dominated by a large, centrally-concentrated structure associated with Totoro, but the peak position of CO is offset toward the south of Hα peak by $\sim 0.3''$ ($\sim$ 200 pc). The multi-wavelength peak coordinates of Totoro, along with other properties that will be derived and discussed in this paper are provided in Table 2. The two arm-like structures connecting the extended structure and the central region of the galaxy are also seen in CO. Moreover, as somewhat expected, an early-type galaxy like Satsuki has a low molecular gas content. While there is a strong and compact Hα emission at the nucleus of Satsuki, no CO detection is found at this position. Instead, two knots are moderately detected in the northeast and southwest of the nucleus. Although their orientation is consistent with that of the possible past AGN jets indicated by X-ray cavities (O'Sullivan et al. 2019), deep CO observations are required to confirm the nature of these two knots.

We cannot rule out that the Hα and CO morphologies would appear more clumpy if the angular resolution is improved. The recently reported size of gas clumps in ram-pressure-stripped tails of galaxies range from several hundreds of parsec to several kpc (e.g., Bellhouse et al. 2017; Lee & Chung 2018; Jáchym et al. 2019; López-Cobá et al. 2020). Although we are not able to resolve individual gas clumps with our $\sim$ 1.7 kpc resolution, if Totoro is intrinsically clumpy as ram-pressured stripped gas, we should see a sign of clumpy sub-structure given that the size of the object is as large as 6 – 8 kpc in diameter.

Ram-pressure-stripped gas is known to have high velocities (several hundreds of km s^{-1}) and velocity dispersions ($>$ 100 km s^{-1}) (e.g., Bellhouse et al. 2017; Consolandi et al. 2017). Figure 3c and 3d display the CO and MaNGA Hα velocity fields in color scale. For ease of comparison, contours of CO integrated intensity map are overplotted on both velocity fields. There is a strong variation in the line of sight Hα velocity at the two connecting arms, with redshifted gas in the left tail and blueshifted gas in the right tail. Such features are not observed in the CO velocity field. At the main blob region of Totoro, both CO and Hα velocity field show no velocity gradient, little variation, and low velocity (mostly $\leq$ 60 km s^{-1}) across the region, suggesting that the system is not in rotation, unless it is perfectly face-on. The velocity dispersion of Hα gas in the region of Totoro is only $\sim$ 50 km s^{-1} (Paper I); the narrow CO line width also implies a low gas velocity dispersion. Therefore, the gas kinematics of Totoro is in conflict with that of ram-pressure stripped gas. We should caution, however, that the velocity resolutions of our CO and Hα map are relatively low, $\sim$ 50 and 70 km s^{-1}, respectively. Further observations are needed to probe the detailed kinematics of Totoro.

Moreover, if ram-pressure stripping is the main origin of Totoro, the molecular-gas data imply that the cold gas is stripped almost completely from Satsuki. However, such a scenario is disfavored by simulations of ram-pressure stripping (Steinhauser et al. 2012, 2016). A galaxy can lose all of its gas only in extreme cases of ram-pressure stripping, e.g., galaxy encounters high ICM densities with very high relative velocity. In addition, massive galaxies, are less prone to lose their gas due to ram-pressure stripping because the existence of a massive bulge can prevent the stripping of gas and reduce the amount of gas being stripped. Finally, galaxies that show ram-pressure stripping are mostly gas-rich late-type galaxies (Poggianti et al. 2017, and series of papers by the GAs Stripping Phenomena in galaxies with MUSE, GASP, team). For these reasons, the CO and Hα gas are unlikely to be moved from the center of Satsuki to the current position as a result of ram-pressure stripping. However, we note that this does not mean that the galaxy has not experienced any ram-pressure stripping. We come back to this discussion in Section 3.4.3.

3.2. *Separate Galaxy*

In Paper I, we argue that Totoro may be a separate galaxy interacting with the dry merger (Satsuki and Mei). We can examine this scenario by (1) searching for its underlying stellar component; (2) looking for interaction features; and (3) comparing the molecular gas and star formation properties of this galaxy candidate with other galaxy populations.

3.2.1. *Underlying Stellar Counterpart*

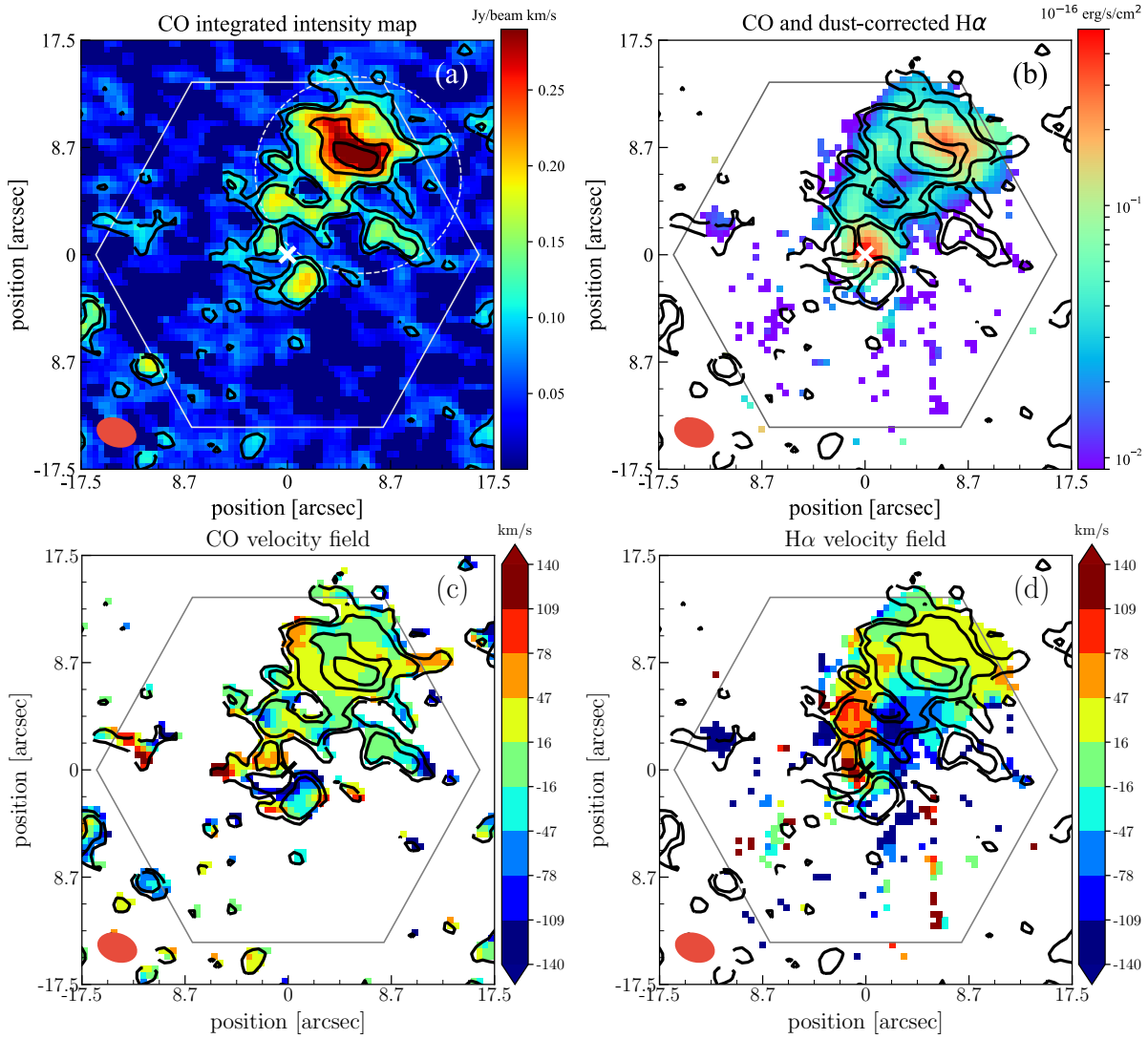

Figure 3. (a) Map of ^{12}CO(1-0) integrated intensity map (color and contours) with the MaNGA hexagonal FoV overlaid. The ^{12}CO contours are in intervals of 2, 3, 5.5, and 7.5σ, where 1 σ corresponds to 40 mJy beam^{-1} km s^{-1}. The nucleus of Satsuki is marked with a white cross. The synthesized beam (3.4″ × 2.34″, PA = 73.3°) is plotted in the bottom left. The dashed ellipse indicates the area we have used for generating the integrated spectrum in Figure 2. (b) Similar to the panel (a), but the color map shows the Hα emission from the MaNGA survey. (c) Velocity field of gas traced by ^{12}CO(1-0) (color scale), with ^{12}CO(1-0) intensity contours overlaid. (d) Velocity field of gas traced by MaNGA Hα (color scale). The contours are the same as in other panels.

The CFHT u-, g-, r, and i-band images are presented in Figure 4a – 4c, respectively. There are extended stellar halos surrounding the two galaxies, but we find no apparent optical counterpart directly from the images at the position of Totoro. The limiting magnitude[6] and the surface brightness of Totoro are listed in Table 3. Due to the absence of an optical counterpart at the position of Totoro, only upper limits can be placed on surface brightnesses (i.e., limiting surface brightness of the observations).

In Paper I, we used a multi-component GALFIT (Peng et al. 2010) model for searching for a stellar component of Totoro from a g-band image and found no substructure that is responsible for the blob. However, the residual of this complex parametric model still showed significant fluctuations that could hinder the detection of small scale sub-structure (see Figure 6 in Paper I). The on-going interaction of the main system creates an extended stellar envelope and asymmetric structures

[6] The *gri* limiting surface brightnesses quoted here are different from that given in Paper I. This is because the former is scaled from the limiting magnitudes using 1″ aperture size while the latter was measured using an aperture size corresponding to one arcsec^2 area, which however is more affected by the Point Spread Function (PSF) because of the small aperture.

Table 2. Properties of the offset-cooling gas Totoro.

General Properties	
host	VII Zw 700 (dry merger: Satsuki and Mei)
redshift[a]	0.0322
distance to the host	$\sim$ 8 kpc
enviroment	merging group
Peak Position[b]	
^{12}CO(1-0)	17:15:22.46, +57:26:6.90
Hα[c]	17:15:22.40, +57:26:7.83
X-ray	17:15:22.52, +57:26:7.89
Luminosity	
^{12}CO(1-0)	4.8×10^7 K km s pc^2
Hα[c]	5.9×10^{39} erg s^{-1}
X-ray	4.4×10^{40} erg s^{-1}
Gas Mass	
cold gas (H_2)	2.1×10^8 M$_\odot$ (^{12}CO (1-0))
	1.9×10^8 M$_\odot$ (A_V: cloud)
	2.5×10^8 M$_\odot$ (A_V: diffuse)
warm gas (Hα)	8.2×10^4 M$_\odot$
hot gas (X-ray)	1.2×10^9 M$_\odot$
Other Properties	
SFR[d]	< 0.047 M$_\odot$ yr^{-1}
cooling time	2.2×10^8 yr

[a] Redshift of VII Zw 700, taken from the NASA-Sloan Atlas (http://nsatlas.org/).
[b] Position of intensity peak in images, no centroid fitting is performed.
[c] Based on MaNGA Hα data.
[d] Based on the assumption that all MaNGA-Hα fluxes come from star formation.

that are challenging to the model. In this paper, we use three different approaches to further search for a potential stellar counterpart to Totoro from multiple-band (g, r, and i) images. All three methods are commonly used in literature for background subtraction and for both compact and extended source detection.

Table 3. The 5σ limiting magnitudes of CFHT u-, g-, r-, and i-band images and the 5σ upper limit of the surface brightness of Totoro at each band.

band	limiting magnitude ($1''$ radius) [mag]	surface brightness of Totoro (upper limit) [mag arcsec^{-2}]
u	26.3	27.54
g	25.7	26.94
r	26.2	27.44
i	25.2	26.44

Firstly, we use the Python photometry tool `sep` (Barbary et al. 2016)[7] to generate a "background" model of the image with small background box size (5 pixels). The tool `sep` uses the same background algorithm as in `SExtractor` (Bertin & Arnouts 1996). We then subtract the "background" model from the image to increase the contrast around the main galaxies. This method has been used to separate galaxy stellar halos and the light from adjacent (background) objects (e.g., Huang et al. 2018; Rubin et al. 2018), and to identify faint, extended emission such as tidal tails (e.g., Mantha et al. 2019).

As a second approach, we subtract a blurred version of the image from the original one. The blurred version of the image is created by convolving the image with a circular Gaussian kernel (σ = 4 pixels). This procedure is part of the unsharp masking method in digital image processing[8] and can also increase the contrast of the image. Compared to the first approach, the Gaussian convolution makes it more sensitive to a low threshold feature with a sharp edge. This method has been commonly used to identity HII regions in galaxies (e.g., Rahman et al. 2011; Pan et al. in preparation) and to detect faint embedded spiral and bar features in early-type galaxies (e.g., Barazza et al. 2002; Kim et al. 2012). The method has been applied to IFS data for the later purpose as well by Gomes et al. (2016).

For our third method, we perform isophotal fitting using the `Ellipse` task in `IRAF` (Tody 1986, 1993). We first mask out all detected objects other than the main galaxy using `sep`. Then we run `Ellipse` on the masked images, allowing the centroid and the shape of the isophote to vary. Using the resulting isophotal parameters, we create the corresponding 2-D model using the `bmodel` task and subtract it from the input image. Compared to the `GALFIT` parametric model, the `Ellipse` one does not depend on the choice of model component and typically leads to smoother residuals. This approach has been routinely used to determine morphology of elliptical and lenticular galaxies (e.g., Hao et al. 2006; Oh et al. 2017) and to search for low-surface-brightness tidal features in nearby galaxies (e.g., Tal et al. 2009; Gu et al. 2013).

The residual maps of these methods are shown in Figure 5. From left to right the panels correspond to the analysis of the background, unsharp mask, and isophotal fitting methods; from top to bottom we show the residual maps and annular residual profiles of u-, g-,

[7] https://github.com/kbarbary/sep
[8] The original unsharp mask technique re-scales the residual and add it back to the original image.

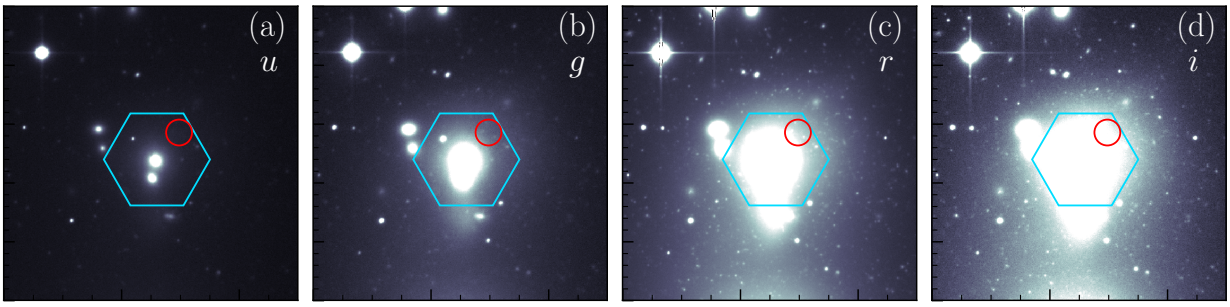

Figure 4. CFHT u-, g-, r-, and i-band images (from left to right). The first three bands combine archival data downloaded from the CADC server and the data taken in 2015 summer (see Paper I for the details). The u-band data was taken later in 2017. The cyan hexagon and red circle mark the region of MaNGA FoV and the Hα blob Totoro.

r- and i-band, respectively (u-band results will be discussed later in this section). The annular profiles are centered on the Hα peak of Totoro. We also explore different parameters adopted in these procedures (e.g., the size of the background box or the convolution kernel). The choice of these parameters within a reasonable range does not affect the results.

Using these methods, we detect a large number of unresolved (point-like) sources on the g-, r- and i-band images, presumably a combination of globular clusters of the main system and background galaxies. The residual profiles are generally flat, fluctuating around the zero value. This is true for all gri bands and methods, suggesting that there is no sign of a distinctive stellar counterpart at the position of Totoro. Therefore, our new analyses confirm the previous result by using GALFIT in Paper I. There are two unresolved sources in the Totoro area (red circle in Figure 5), but we do not notice any increase or decrease of number density around the Totoro area. The two sources are associated with neither Hα nor CO peak. We will come back to the nature of these two unresolved sources later. On the residual maps from the unsharp mask method, we uncover a pair of "ripple"-like features close to the center of the main galaxy. These sub-structures remain the same when we vary the convolution kernel used, and they resemble the structure we saw on the GALFIT residual maps in Paper I. Such "ripples" often relate to recent galaxy interaction or the presence of dust (e.g., Colbert et al. 2001; Kim et al. 2012; Duc et al. 2015; Bílek et al. 2016). However, it is unclear whether there is any connection between them and Totoro.

Since there is no optical (g, r, and i) continuum counterpart found in Totoro, it is expected to be composed mostly of young stars if it is indeed a galaxy. In Paper I, we use the excitation state of optical lines to constrain the presence of young stars. However, the result is method (diagnostic diagram) dependent. The u-band luminosity of a galaxy is dominated by young stars of ages < 1 Gyr, therefore it is more sensitive to any recent star formation than any of the other broad band luminosities available (Moustakas et al. 2006; Prescott et al. 2009; Zhou et al. 2017), and is a more straightforward probe than optical emission line diagnostics.

Similar to the gri bands, the u-band emission in the MaNGA hexagonal FoV is dominated by the dry merger (Satsuki and Mei) as shown in Figure 4, but the u-band data is less affected by the large stellar halos associated with the dry merger (Satsuki and Mei) than the redder bands, and therefore serves as a better probe for underlying stellar component. The limiting magnitudes and surface brightness of the u-band image are 26.3 mag and 27.54 mag arcsec^{-2}, respectively (Table 3). The point source in the upper-left corner of the dry merger (Satsuki and Mei) is a foreground star according to the MaNGA spectrum.

Although visually there is no distinguishable u-band feature (i.e., recent star formation) associated with Totoro, to ensure that the u-band counterpart of Totoro is not embedded within the light of the dry merger (Satsuki and Mei), we subtract the photometric models for the merging system from the u-band image using the three different methods mentioned above. The residual maps and profiles are shown in the top row of Figure 5, respectively. The residual maps and profiles are not perfectly smooth, but we find no obvious evidence for a distinctive, extended u-band counterpart at Totoro. The two point sources seen in g-, r-, and i-band residual maps are also seen in the u-band residual image of the isophotal fitting (and marginally seen in the background method as well). This confirms the results in Paper I that star formation alone can not explain the excitation state of Totoro.

To gain some insight into the nature of the two unresolved objects in the Totoro area, their photometric redshifts are determined using the EAZY (Brammer et al. 2008) and PÉGASE 2.0 (Fioc & Rocca-Volmerange 1997) template fitting the aperture magnitudes measured from the isophotal fitting residual images using GAIA (Graphical Astronomy and Image

Analysis Tool). The default EAZY template is generated from the PÉGASE 2.0 models using the Blanton & Roweis (2007) algorithm and then calibrated using semi-analytic models, plus an additional young and dusty template. The PÉGASE 2.0 template is a library including ∼3000 models with a variety of star formation histories and with ages between 1 Myr and 20 Gyr, as described in detail in Grazian et al. (2006). Figure 6 shows the chi-squared of the fit for a given redshift us-

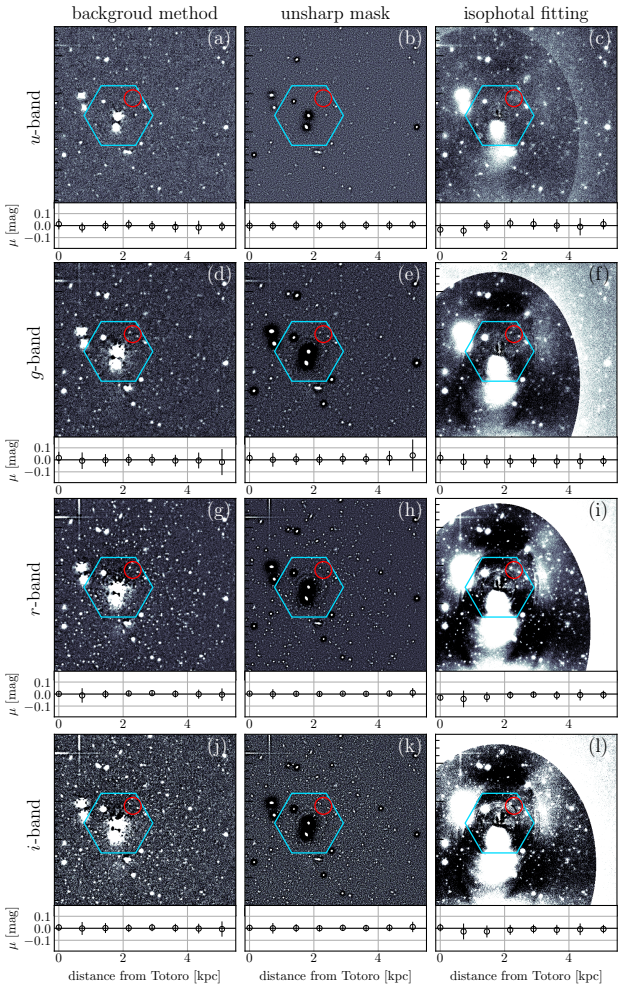

Figure 5. The residual images and annular residual profiles after subtracting the model images of the dry merger (Satsuki and Mei). The annular profiles are centered on the Hα peak of Totoro. Three different approaches (from left to right: background method, unsharp mask, and isophotal fitting) are used to search for distinctive stellar counterpart and star formation of Totoro on the u-, g-, r- and i-band images (from top to bottom). The cyan hexagon and the red circle mark the regions of MaNGA FoV and Totoro, respectively. We do not observe a significant, extended stellar component around with Totoro in any residual maps and profiles. There are two point sources around the position of Totoro, they are likely background sources (see text for the details).

ing the EAZY and PÉGASE templates (left column of each panel) and the best-fit SED with observed fluxes at i-, r-, g- and u-band overlaid as red circles (right column of each panel). The results based on the EAZY and PÉGASE templates are presented in the top and bottom rows respectively. The minimum chi-squared value indicates that the southern source ($17^{\rm h}15^{\rm m}22.111^{\rm s}$, $+57°26'5.628''$) is a background galaxy at $z \sim 0.40$ and 0.37 using the EAZY and PÉGASE templates, respectively (Figure 6a). The redshift of our target is marked by a yellow dashed line in the figures. We notice a second minimum at $z < 0.03$, close to the redshift of our target. However, at such low redshifts, the source would be resolved, not point like. The most plausible redshift of the northern source ($17^{\rm h}15^{\rm m}22.573^{\rm s}$, $+57°26'7.659''$) is 0.29 according to both templates (Figure 6b), but we cannot rule out other possibilities of $z < 0.4$, in particular $z \sim 0.15$, due to the shallower basin-shaped chi-square distribution. Nonetheless, the redshift of Totoro (yellow dashed line) is not associated with any local minimum of the chi-square values. We find poorer fits when using stellar templates, providing further support that the source is not a nearby object. The best-fitted SEDs from PÉGASE are exported to SED-fitting code `New-Hyperz`[9] in order to derive the stellar mass (M_*) and star formation rate (SFR) of these two objects. The results suggest that the southern and northern sources are $\sim 3 \times 10^8$ and $\sim 6 \times 10^8$ $M_\odot$ and their specific SFR (sSFR = SFR/M_*) are $\leq 10^{-11}$ yr^{-1}. We also estimate their M_* assuming they are at the same redshift as Totoro ($z = 0.03$), and yield $\sim 10^6$ and $\sim 10^7$ $M_\odot$ for the southern and northern sources, respectively. Given their point-like morphologies (< 1 kpc^2), we expect to see distinctive stellar mass surface density (Σ_*) distributions in the MaNGA data if they are associated with Totoro. However, we find no such features. It should be noted that the above stellar masses may be subjected to non-negligible uncertainties due to the lack of (near-) infrared measurements.

We use web interface Marvin[10], a tool to visualise and analyse MaNGA data (Cherinka et al. 2019), to search for any signatures in the spectra of these two sources by redshifting strong optical emission lines (e.g., Hα) based on the derived photometric redshifts. However, the emission lines are too faint to be seen by MaNGA. Given their likely high redshift and their positions being offset from the centroid of the Hα blob, these two point sources are unlikely to be associated with Totoro.

[9] http://userpages.irap.omp.eu/~rpello/newhyperz/
[10] https://dr15.sdss.org/marvin